



# 1 Preliminary Techno-Economic Study of Optimized Floating 2 Offshore Wind Turbine Substructure

3 Adebayo Ojo<sup>1,\*</sup>, Maurizio Collu<sup>1</sup>, Andrea Coraddu<sup>2</sup>

4 <sup>1</sup>Department of Naval Architecture Ocean and Marine Engineering, University of Strathclyde, Glasgow G4  
5 0LZ, UK; adebayo.ojo@strath.ac.uk; maurizio.collu@strath.ac.uk

6 <sup>2</sup>Department of Maritime & Transport Technology, Delft University of Technology, 2628 CD Delft, The  
7 Netherland; a.coraddu@tudelft.nl

8  
9 \*Correspondence to: Adebayo Ojo (adebayo.ojo@strath.ac.uk)

---

## 11 Abstract

12 Wild fires and excessive floodings have been seasonal climatic changes across the globe in the past decade. The  
13 need for clean energy to fight against the climate changes observed as a result of excessive green-house emission  
14 over the years is driving the development of the offshore wind sector. This drive is pushing the exploitation of  
15 rich wind resources in deep waters with water depth greater than 60 metres requiring a deviation from the  
16 commercialized fixed bottom foundation offshore wind technology. Resolving the issue of exploiting rich wind  
17 resources requires the use of floating foundation offshore wind technology satisfying stability and durability  
18 requirement in any environmental condition.

19 Floating offshore wind turbines (FOWTs) are still in the pre-commercial stage and although different concepts of  
20 FOWTs are being developed, cost is a main barrier to commercializing the FOWT system. This is evidence in  
21 the comparison of the CAPEX (capital expenditure) for a fixed bottom platform and a floating platform with the  
22 fixed bottom foundation CAPEX representing 13.5% of the total CAPEX of the system while the floating platform  
23 CAPEX represents about 29% of the total CAPEX of the system leading to an increasing cost.

24 This article aims to use a shape parameterization technique within a multidisciplinary design analysis and  
25 optimization framework to alter the shape of the FOWT platform with the objective of reducing cost. This cost  
26 reduction is then implemented in a 30 MW floating offshore wind farm (FOWF) designed based on the static pitch  
27 angle constraints (5 degrees, 7 degrees and 10 degrees) used within the optimization framework to estimate the  
28 reduction in the levelized cost of energy (LCOE) in comparison to a FOWT platform without any shape alteration  
29 – OC3 spar platform design. The optimal platform design variants and the OC3 platform are also deployed in a  
30 scaled up 60 MW farm to see the impact of platform geometric shape optimization in a scaled-up scenario.

31 Key finding in this work shows that an optimal shape alteration of the platform design that satisfies the design  
32 requirements, objectives and constraints set within the MDAO framework contributes to significantly reducing  
33 the CAPEX cost and the LCOE in the 30 MW floating wind farm. This is due to the reduction in the required  
34 platform mass for hydrostatic stability when the static pitch angle is increased. The FOWF designed with a 10  
35 degrees static pitch angle constraint provided the lowest LCOE value while the FOWF designed with a 5 degrees  
36 static pitch angle constraint provided the largest LCOE value barring the FOWT designed with the OC3 dimension  
37 which is over designed and over dimensioned. The total cost and LCOE is further reduced in a scaled up 60 MW  
38 farm for each design assessed. This further reduction is due to combination of the geometric shape  
39 parameterization and optimization of the platform with the economics of scale of the wind farm.

40  
41 Keywords: FOWT; MDAO; shape parameterization; CAPEX; fixed bottom

---

42  
43  
44  
45  
46  
47  
48  
49  
50  
51  
52  
53  
54



### Abbreviations

AEP	Annual Energy Production
B-Spline	Basis Spline
CAPEX	Capital Expenditure
DECEX	Decommissioning Expenditure
DPBP	Discounted Pay Back Period
DNV	Det Norske Veritas
GBP	Great British Pounds
GWh	Giga Watts Hour
FOWF	Floating Offshore Wind Farm
FOWT	Floating Offshore Wind Turbine
IRR	Internal Rate of Returns
LCOE	Levelized Cost of Energy
MDAO	Multidisciplinary Design Analysis and Optimization
MW	Mega Watts
MWh	Mega Watts Hour
NPV	Net Present Value
OC3	Offshore Code Comparison Collaboration
OPEX	Operating Expenditure
OWT	Offshore Wind Turbine
PSM	Pattern Search Model
TLP	Tension-Leg Platform
WACC	Weighted Average Capital Cost
WADAM	Wave Analysis by Diffraction and Morison Theory

55  
56  
57  
58  
59  
60  
61  
62  
63  
64  
65  
66  
67  
68  
69  
70  
71  
72  
73  
74  
75  
76  
77  
78  
79  
80  
81  
82  
83  
84  
85  
86  
87  
88



89

## 1. Introduction and Background

90 With more than three-quarter of the world's offshore wind resource potential available in waters deeper than  
91 60m along the coastline of many countries, the potential for fixed bottom offshore wind system becomes limited  
92 (Gwec, 2022). This highlights the need for Floating Offshore Wind Turbine (FOWT) technology in order to see  
93 a true global growth of the clean technology (FOWT) to contribute to the reduction in green house emission.

94 Mega-Watts' (MW) scale floating technologies have only been tested in the last ten years through  
95 demonstration and pilot projects in both Europe and Asia. With the completion of the demonstration projects,  
96 deployment of floating offshore wind turbine system has not entered the commercial or industrial phase as  
97 development has just entered the pre-commercial stage with a shift in emphasis moving towards a larger first of  
98 a generation schemes(Gwec, 2022). It is anticipated that 2026 FOWT system deployment will move into the  
99 commercial phase with yearly installations surpassing 1 GW – a milestone achieved by fixed offshore wind in  
100 2010 (Dnv-GI, 2020).

101 The concept of floating offshore wind turbine has been conceived since the 1970s (Heronemus, 1972). Despite  
102 the early conception, FOWT is still in the pre-commercial stage leaving the fixed bottom foundation/platform in  
103 the dominant technology in the offshore wind turbine (OWT) sector (Zheng and Lei, 2018). The most efficient  
104 offshore foundations are floating offshore wind platforms because of all the advantages they offer. First and  
105 foremost, they enable the exploitation of huge sections of ocean that are deeper than 60 metres. Second, they make  
106 it easier to set up turbines, even in mid-depth circumstances (30–50 m), and they might eventually present a less  
107 expensive option than solid foundations. FOWT technology provides the capability to move further offshore to  
108 exploit better wind resources while also limiting visual impact from land and away from competing with other  
109 users of the sea (Kaldellis et al., 2016). Additionally, due to less invasive construction methods on the seabed than  
110 fixed-bottom designs, floating foundations typically provide environmental advantages over them. The world's  
111 forecast growth of floating offshore wind was 17MW in 2020 to 6.5GW by 2030. A review of the forecast was  
112 conducted in 2021 with the forecast increased to 16.5GW of floating offshore wind capacity by 2030 (Gwec,  
113 2022) highlighting a significant interest in increasing the capacity of the FOWT technology in reducing the green-  
114 house emission. The floaters required for offshore wind must provide adequate buoyancy to support the weight  
115 of the wind turbines and also have the capability to constrain the motions within allowable limit (Butterfield et  
116 al., 2007).

117 Three main floating platform concepts (spar, semisubmersible, and tension leg platform) from the oil and gas  
118 industry are the early adapters (early to market floaters) in the FOWT sector. The stabilization mechanisms of the  
119 three platforms highlighted are: ballast, waterplane / buoyancy and mooring stabilization respectively. As  
120 highlighted in Leimeister et al. (2018), several floating solutions have currently been developed that are  
121 anticipated to be appropriate and considerably financially viable in depths more than 60 m. These new floating  
122 solutions still adapt the stability mechanisms used in the early adapters floaters from the oil and gas sector.

123 The ballast stabilized spar requires a large ballast that is deep at the bottom of the floater to move the center of  
124 gravity of the system below the center of buoyancy in order to provide a restoring moment or stabilizing righting  
125 moment which counteracts the inclining moments. In the waterplane area or buoyancy stabilized semi-  
126 submersible, a large second moment of waterplane area with respect to the rotational axis creates the restoring  
127 moment to counteract against the rotational displacement. The mooring stabilized TLP utilizes high tensioned  
128 mooring lines to generate the restoring moments to counteract the effect of any inclining moment on the structure.  
129 The benefits and challenges associated with the three types of platforms associated with the stability mechanism  
130 described are highlighted in Table 1 and Table 2 respectively. The choice of the platform used for a FOWT system  
131 will also depend on elements like water depth, localization potential, local infrastructure, and various turbine  
132 designs. As a result, the market will likely adjust to changing situations rather than rationalize around a single sort  
133 of floating platform (Gwec, 2022).

134 The average CAPEX of a floating platform is higher than that of a fixed bottom platform. The floating  
135 substructure of a reference wind power plant accounts for approximately 29.5% of the CAPEX for the project in  
136 contrast to 13.5% for a fixed-bottom reference project (Ioannou et al., 2020). These average values can be  
137 significantly higher or lower depending on the floater type employed and will significantly impact the profitability  
138 of the project. It is expected to see innovation in design, construction, operation and maintenance as the industry  
139 evolves to facilitate the build and operation of larger FOWT projects. The construction of FOWT system can be  
140 in ports or sheltered waters making use of specialized vessels. Major maintenance and repair activities might also  
141 be carried out away from the site using the innovative "tow-to-port" maintenance capability. Continuous  
142 innovation in design is expected to yield new technologies and products capable of supporting better mooring and  
143 anchor solutions, deep water substations and dynamic cabling, management of FOWT system's response to  
144 environmental conditions and sea-states and the design of floating platforms.

145 Bringing the cost of floaters/platform used in the FOWT system down to the level of fixed bottom platform  
146 needs extensive developmental process and ideas exploration. Some of the processes and ideas that can be  
147 explored in driving down the cost of FOWT systems are:



- 148 1. Geometric shape parametric design, analysis and optimization of the FOWT platform (Clauss and Birk,  
 149 1996; Birk and Clauss, 2002; Birk, 2006; Ojo et al., 2022b);  
 150 2. Upscaling design platform to fit with larger and bigger turbines (Leimeister et al., 2016; Kikuchi and  
 151 Ishihara, 2019; Papi and Bianchini, 2022);  
 152 3. Multidisciplinary design analysis and optimization of all components within the FOWT system (Turbine,  
 153 tower, platforms, mooring lines and anchors) (Leimeister et al., 2020a; Karimi et al., 2017; Karimi, 2018);  
 154 4. Provision of government subsidy to floating wind projects in the precommercial stage to add economic  
 155 value until the FOWT technology becomes cost competitive with the fixed-bottom OWTs (Markus Lerch,  
 156 2019).

157 The main aim of this study is to investigate the economic implication of use of bespoke geometric shape  
 158 parameterization, design, analysis and optimization framework of spar platforms on a 30 MW floating wind farm  
 159 and also the cumulative effect of this bespoke approach and economies of scale on a 60 MW floating wind farm.  
 160 This investigation will be conducted with the use of some of the financial parameters highlighted in section 2 in  
 161 conjunction with the methodology discussed in section 3. The techno-economic study highlighting the impact on  
 162 costing is detailed in in section 4 and adequate conclusion presented in section 5.  
 163  
 164

Table 1. Benefits of traditional platforms

Spar	Semi-submersible	TLP
Suitable for severe seastate	Broad weather window for installation	Small seabed footprint and short mooring lines
Inherent stability	Independent of water depth	High stability and low motions
Soil condition insensitivity	Soil condition insensitivity	Have a good water-depth flexibility
Simple fabrication process	Minimal risk to installation and operation	Possibility of onshore or dry dock assembly
Low operational risk	Heave plates for reducing heave response	Lower material cost due to minimal structural weight of the substructure
Little susceptibility to corrosion	Simple installation and decommissioning as specialised vessel required	Simple and light structure, easy for operation and maintenance
Cheap and simple mooring and anchoring system		

165  
 166

Table 2. Challenges of traditional platforms

Spar	Semi-submersible	TLP
Heavy weight with long draft and long mooring lines	Higher exposure to waves leads to lower stability that impacts turbine	High vertical load moorings
Deep drafts limit ports access and large seabed footprint	Labour intensive and long lead time	Unstable during assembly and will require the use of special vessels
Relatively large motions	Large and complex structure – difficult to fabricate	Moorings tendons present higher operational risk in case of mooring failure
Assembly in sheltered deep water is challenging and time consuming	Built in one piece requiring dry dock or special fabrication yard with skid facilities	Complex and costly mooring and anchoring system makes it the most expensive floater design type
High design manufacturing and installation cost.	Lateral movement presents potential problems for the export cables	Additional investigation of seabed condition to ensure it's fit for purpose of high tensioned mooring
High fatigue loads in tower base	Non-industrialized fabrication	
Specialised installation vessel required.		



## 167 2. FOWT Techno-Economic Feasibility Review

### 168 2.1. Overview

169 At the turn of the millennium, the total installed costs for offshore wind farms were evaluated from those of  
170 existing shallow water and extrapolated to deeper waters for deep water offshore farms. The extrapolation resulted  
171 in increased costs of foundations, grid connection and installation. The new farms so designed had the effect of  
172 increasing the average cost of offshore wind installations from 2.300 €/kW in the year 2000 to a peak of 5.0 €/kW  
173 in the period between 2011 and 2014. However, from 2015 the total costs of FOWFs started to decreasing and in  
174 2018, the decrease was down to 4.0 €/kW (Maienza et al., 2022; Irena, 2019a, b)

175 The predicted cost for FOWFs is also expected to decrease, according to recent study, primarily due to  
176 technological advancements. These allow capacity factors to rise while lowering overall installation and  
177 maintenance costs (Maienza et al., 2022). Additionally, the rise in this technology's competitiveness can also be  
178 efficiently improved by the following:

- 179 • Adequate use of shape parameterization technique within the multidisciplinary design analysis and  
180 optimization (MDAO) framework to optimize platforms in accordance to specified design objectives and  
181 constraints;
- 182 • Platform upscaling techniques to bigger and heavier turbines;
- 183 • Increase in designers' experience, which reduces project development costs and risks;
- 184 • The increase in the industry maturity, bringing lower capital cost and;
- 185 • Presence of economies of scale across the value chain.

186 The future development of floating wind technology will benefit from accurate financial analyses sustaining  
187 the economic and technical value of FOWTs. Some of the techno-economic study on FOWTs are detailed herein.

188 Shape parameterization study of the FOWT platform was conducted by Ojo et al. (2022a) to alter the shape of  
189 a spar platform coupled to a 5MW OC3 turbine, reduce the mass of the spar platform leading to a reduction in the  
190 required cost of steel for manufacturing the spar platform. This study used a B-spline parameterization technique  
191 within an MDAO framework with a metaheuristic pattern search optimization algorithm to explore the design  
192 space and produce an optimal design. The optimal design in the study is a spar variant platform with altered shape  
193 and lower mass than the standard OC3 platform. The limitation in this study is that only the cost of steel for the  
194 optimal spar was the only financial parameter to assess the economic feasibility of the FOWT system.

195 Ghigo et al. (2020) conducted a study on platform optimization and cost analysis in a floating offshore wind  
196 farm. This study focuses on the choice of a floating platform that minimizes the global weight, in order to reduce  
197 the material cost, but ensuring buoyancy and static stability. Subsequently, the optimized platform is used to define  
198 a wind farm located near the island of Pantelleria, Italy in order to meet the island's electricity needs. A sensitivity  
199 analysis to estimate the LCOE for different sites is presented, analyzing the parameters that influence it most, like  
200 Capacity Factor, Weighted Average Capital Cost (WACC) and number of wind turbines. The study concluded  
201 that the decrease of many Capex cost items and the evolution of the offshore wind market, will make this  
202 technology even more competitive in a few years.

203 Ioannou et al. (2020) conducted a preliminary parametric techno-economic study of offshore wind floater  
204 concepts. This study investigates through a parametric study the total mass and cost of three floater concepts: spar,  
205 barge and semi-submersible, particularly focusing on the material and manufacturing costs. A survey from floating  
206 offshore wind industry professionals was conducted to determine the manufacturing complexity factors' values,  
207 which were used to calculate the manufacturing cost. The main conclusion of this work is that, given the specified  
208 conditions, steel-based semi-sub structures proved to be the most expensive configuration followed by spar as  
209 spar prices fall with higher draught values due to the reduction in ballast mass. The barge solution is the least  
210 expensive option of the three configurations. Also, the study highlighted the risks and benefits of different  
211 configurations should also be considered alongside, as they could lead to savings throughout the service life of  
212 the asset.

213 Castro-Santos et al. (2016) presented an approach for evaluating the lifecycle costs of combined or a hybrid  
214 floating offshore renewable energy systems like a FOWT. Their methodology expressly takes into account, the  
215 life cycle stages amongst which are: concept generation and definition, design and development, manufacturing,  
216 installation, exploration, exploitation and decommissioning. It is a tool for strategic planning and decision-  
217 making, allowing for a better understanding of technical advancements and factors that could either expedite or  
218 slow down the growth of the FOWT sector. Their findings from two sites show that the exploitation,  
219 manufacturing and installation costs are the most important lifecycle costs on the LCOE but the important of the  
220 three costs could be site dependent.

221 Martinez and Iglesias (2022) conducted an extensive study that mapped the Levelized Cost of Energy (LCOE)  
222 for floating offshore wind in the European Atlantic. They emphasized the importance of understanding LCOE  
223 spatial variations to identify suitable areas for the development of Floating Offshore Wind Turbine (FOWT)  
224 technology. The study focused on floating semi-submersible platforms, presenting a comprehensive LCOE



225 mapping across the European Atlantic. Accurate energy production estimates were obtained by combining  
226 hindcast wind data and an exemplary wind turbine's power curve. The study revealed the lowest LCOE values  
227 (around 95 €/MWh) in wind-rich regions like Great Britain, Ireland, the North Sea, and NW Spain. In contrast,  
228 higher LCOE values (approximately 125 €/MWh) were observed off Portugal and Norway, and significantly  
229 higher values exceeding 160 €/MWh were noted in the Gulf of Biscay and south of the Iberian Peninsula.

230 Filgueira-Vizoso et al. (2022) evaluated the technical and economic viability of floating offshore wind  
231 platforms. Their work defined an economic assessment approach for TLP platform-based offshore wind farms.  
232 Life-cycle costs were categorized into stages including conception, design, manufacturing, installation,  
233 exploitation, and dismantling. Economic indicators like IRR, NPV, DPBP, and LCOE were assessed based on  
234 cash flows. The study focused on a TLP platform designed by CENTEC, considering an 880 MW farm located  
235 along the European Atlantic Coast in the North-West region of Galicia, Spain. Eighteen case scenarios were  
236 analyzed, varying electric tariffs and capital costs. The study underscored the impact of electric tariffs on  
237 economic indicators. The optimal outcome emerged for a tariff of EUR 150/MWh and a 6% cost of capital,  
238 yielding an IRR of 18.34%, NPV of EUR 2636.45 million, and DPBP of 8 years. The farm's LCOE reached a  
239 minimum of EUR 54.33/MWh, rendering the platform economically feasible due to its IRR surpassing capital  
240 costs.

241 Pham and Shin (2019) introduced a novel conceptual design for a spar-type platform, intended to accommodate  
242 a 5 MW offshore wind turbine. This innovative concept effectively addresses challenges associated with the OC3-  
243 hywind model, notably the elevated nacelle acceleration and tower-base bending moment. This achievement is  
244 accomplished through the incorporation of an open moonpool positioned at the platform's center. By leveraging  
245 the water column within the moonpool, the mass and inertia of the entire wind system are augmented along the x  
246 and y axes. By appropriately sizing the moonpool diameter, it becomes possible to mitigate nacelle acceleration  
247 and tower-base bending moment concerns

248 Campos et al. (2016) presented a groundbreaking approach to achieving a cost-efficient offshore wind turbine  
249 floating platform. This novel concept revolves around a monolithic floating spar buoy design. The innovation lies  
250 in the integration of both the tower and floater components as a seamless, continuous concrete structure. This  
251 concept promises significant cost savings, not only during the construction phase but also throughout the  
252 platform's operational lifespan. The inherent design translates to minimal maintenance requirements.  
253 Comprehensive insights into the construction and installation processes are provided in Campos et al. (2016)  
254 considering the distinctive demands of the monolithic design. The authors conducted a comparative analysis of  
255 costs between steel and equivalent concrete platform designs and their findings underscore a material cost  
256 reduction exceeding 60% for the concrete design, reinforcing its economic viability.

257 (Lerch et al., 2018) conducted a study exploring three platform concepts (spar, semi-submersible and TLP) for  
258 floating offshore wind turbines (FOWTs), situated across different locations and comprising a 500 MW floating  
259 offshore wind farm. Their findings underscore the competitiveness of FOWTs, demonstrating their capacity to  
260 generate energy at an equivalent or lower Levelized Cost of Energy (LCOE) compared to bottom-fixed offshore  
261 wind technologies. They identified significant parameters influencing the LCOE FOWF with potential for  
262 substantial cost reductions. Notably amongst these parameters are manufacturing-related costs, including those of  
263 the wind turbine, substructure, and mooring system. These parameters are key factors driving LCOE variations  
264 across all concepts and offshore sites. They also highlighted innovative ideas such as dedicated construction and  
265 assembly facilities tailored for floating wind can further contribute to cost reduction, particularly during the  
266 manufacturing phase of a FOWF components.

267 Castro-Santos et al. (2020a) Castro et al. developed a method to assess the economic viability of deep-water  
268 offshore wind farms by considering their economic factors. This procedure involves the use of various economic  
269 parameters, including internal rate of return, net present value, and levelized cost of energy. Notably, the research  
270 indicated that among the considered platform types, the semisubmersible platform exhibited the most favourable  
271 levelized cost of energy (LCOE) value, followed by the spar platform and the TLP platform.

272 Some innovative studies to improve the design and optimization of floaters also contributes to the process of  
273 maturing the FOWT technology and making it as economically competitive as the fixed bottom foundation  
274 counterpart. Some of the innovative technical and optimization studies are highlighted herein: -

275 Hall et al. (2013) focused on optimizing the hull shape and mooring lines of FOWTs across various  
276 substructure categories. This optimization was carried out using a Genetic Algorithm (GA) and a frequency  
277 domain model based on FAST software. Their model is a linear representation of hydrodynamic viscous damping  
278 and did not include a representation of wind turbine control. The GA was employed for both single and multi-  
279 objective optimization. The study's outcomes revealed an un-conventional design, highlighting the need for further  
280 refinement of cost functions in the optimization process.



281 Karimi et al. (2017) enhanced the research conducted by Hall et al. (2013) by implementing a new optimization  
282 algorithm and a linearized dynamic model, leading to improved optimal solutions. In their study, Karimi et al.  
283 (2017) introduced a fully coupled frequency domain dynamic model and a design parameterization approach. This  
284 allowed for the evaluation of system motions and forces in scenarios involving turbulent winds and irregular  
285 waves. Furthermore, they employed the Kriging-Bat optimization algorithm, a surrogate-based evolutionary  
286 approach, to facilitate the exploration and exploitation of optimal designs across three stability classes of  
287 platforms: MIT/NREL TLP, OC3-Hywind Spar, and OC4-DeepCwind semi-submersible platforms. This  
288 optimization primarily aimed to assess the cost implications of platform stability, as reflected by the nacelle  
289 acceleration objective function, across these three categories of Floating Offshore Wind Turbines (FOWT)  
290 platform stability. This study shows an enhanced correlation between cost and substructure design compared to  
291 the previous work by Hall et al. (2013).

292 Hegseth et al. (2020) conducted a comprehensive design optimization for an integrated system including the  
293 platform, tower, mooring system, and blade pitch controller for a 10 MW spar-type floating wind turbine. The  
294 study involved optimizing various design parameters for the spar, including its diameter and wall thickness along  
295 ten distinct sections. These dimensions, along with the configuration of stiffeners, were represented using a B-  
296 spline curve, utilizing four control points. The study's findings revealed that the optimized platform exhibits a  
297 relatively small diameter within the wave zone and assumes an hourglass shape beneath the waterline. This  
298 particular design serves to minimize wave-induced loads on the structure. Additionally, the distinctive shape  
299 enhances the system's restoring moment and natural frequency in pitch, resulting in an enhanced dynamic response  
300 within the low-frequency spectrum.

301 Dou et al. (2020) introduced an optimization framework tailored for the support structure of floating wind  
302 turbines, specifically the spar-buoy floater, which also includes the mooring system. This framework is developed  
303 from frequency domain modelling, and it extends its analytical capabilities to provide design sensitivities for  
304 various design criteria. This unique capability facilitates rapid optimization by leveraging on the Sequential  
305 Quadratic Programming (SQP) optimization algorithm.

306 The optimization techniques discussed in Hall et al. (2013); Karimi et al. (2017); Hegseth et al. (2020) and  
307 Dou et al. (2020) also reviewed above have the capability of reducing the computational time for the design and  
308 analysis of FOWTs. The reduction in time to search a large design space and identify optimal solutions allows  
309 stakeholders in making informed decisions that can potentially help in driving down the cost of FOWT to the  
310 levels of cost in fixed bottom foundation turbines.

311 This study aims to further reduce computational time for design of bespoke FOWTs and also reduce the LCOE  
312 of a FOWF by integrating shape parameterization techniques using B-spline parametric curve to model a spar.  
313 The design and analysis process of the spar is integrated with a gradient free optimizer to search the design and  
314 analysis space and select the optimal design in a quick duration.

## 315 2.2. Financial Parameters

### 316 2.2.1. Net Present Value

317  
318 The Net Present Value (NPV), corresponds to the net value of the cash flows of the floating offshore wind farm,  
319 taking into account its discount from the beginning of the investment (Castro-Santos et al., 2016; Castro-Santos  
320 et al., 2020b). It is dependent on the cash flow in year  $t$ ,  $CF_t$ , the discount rate ( $r$ ) and the initial investment  $G_0$ , as  
321 highlighted in Eq. (1).  
322

$$NPV = -G_0 + \sum_{t=1}^n \frac{CF_t}{(1+r)^t} \quad (1)$$

323  
324 The discount rate ( $r$ ) considered for a project is the WACC (weighted average cost of capital) (Filgueira-Vizoso  
325 et al., 2022). Investment decisions made from the NPV's are highlighted herein.

- 326 • NPV > 0. The investment will generate earnings above the required return ( $r$ ). This will imply that the  
327 acceptance of the project is recommended
- 328 • NPV < 0. The investment produces returns below the required minimum return ( $r$ ). It is not recommended  
329 to accept the project.
- 330 • NPV = 0. The project does not add monetary value above the required profitability ( $r$ ).

331 The decision must be based on other criteria such as obtaining a better position in the market.  
332  
333



### 333 2.2.2. Internal Rate of Return

334

335 The internal rate of return (IRR) is the interest generated by the project throughout its useful life. This is defined  
336 as the discount rate that cancels the NPV. It is the interest rate that makes the future flow of funds financially  
337 equivalent to the initial outlay (Filgueira-Vizoso et al., 2022). The IRR is highlighted in Eq. (2).  
338

$$-G_0 + \sum_{t=1}^n \frac{CF_t}{(1 + IRR)^t} = 0 \quad (2)$$

339

340 The economic feasibility of the project will depend on the IRR and profitability can be defined from the three  
341 conditions highlighted herein.

342

- 343 • IRR < k. The profitability obtained from the project is less than the required minimum. This shows the  
344 investment is not recommended.
- 345 • IRR > k. The profitability of the project is above the required minimum, therefore, it is recommended to  
346 invest in the project.
- 347 • IRR = k. The profitability is the same as that required minimum, the same happens as in the case where  
348 the NPV = 0. The decision in this kind of scenario is conditioned by other factors

### 349 2.2.3. Discounted Pay-Back Period

350

351 The discounted pay-back period (DPBP), in years, comprises the cash flow of each year with the respective  
352 discount rate and adds it to all the previous cash flows with their respective discount rate, accumulating its NPV  
353 (Filgueira-Vizoso et al., 2022). When this sum is equal to or greater than the initial investment, this is the year of  
354 the DPBP, as highlighted in Eq. (3). The best DPBP is as low as possible.  
355

$$\sum_{t=1}^n \frac{CF_t}{(1 + r)^t} \geq G_0 \quad (3)$$

356

357 The feasibility of the project is assessed by the conditions highlighted herein.

358

- 359 • DPBP <<< t. The initial outlay takes less time to recover than the life of the project (t). It is recommended  
360 to accept the project in this scenario.
- 361 • DPBP = t. The initial outlay takes to recover the same as the life of the project (t). This highlights the  
362 project is indifferent or no changes in project.
- 363 • DPBP > t. The initial outlay takes longer to recover than the life of the project (t). It is recommended to  
364 reject the project in this scenario.  
365

### 366 2.2.4. LCOE

367

368 The levelized cost of energy (LCOE) is theoretically the price at which the electricity would have to be sold to  
369 reach the break-even point. It is therefore a fundamental parameter in analysing the economic viability of an  
370 energy project and serves as a standardised approach to compare costs of different energy sources (Martinez and  
371 Iglesias, 2022) – onshore/offshore wind, solar, coal, hydro. The LCOE can be defined as the ratio of the costs of  
372 an energy project to the electricity production over its lifetime, which is usually expressed as highlighted in Eq.  
373 (4).  
374

$$LCOE = \frac{\sum_{t=1}^n (CAPEX_t + OPEX_t)(1 + r)^{-t}}{\sum_{t=1}^n (AEP_t)(1 + r)^{-t}} \quad (4)$$

375

376 where the costs are subdivided into CAPEX (capital expenditures), i.e., the costs spent prior to the operation of  
377 the project, and OPEX (operational expenditures), i.e., the costs of the electricity production and maintenance of  
378 the energy farm. AEP represents the annual energy production of the project, which constitutes the main source  
379 of income. The variable t represents the lifetime of the project in years and r denotes the discount rate.  
380

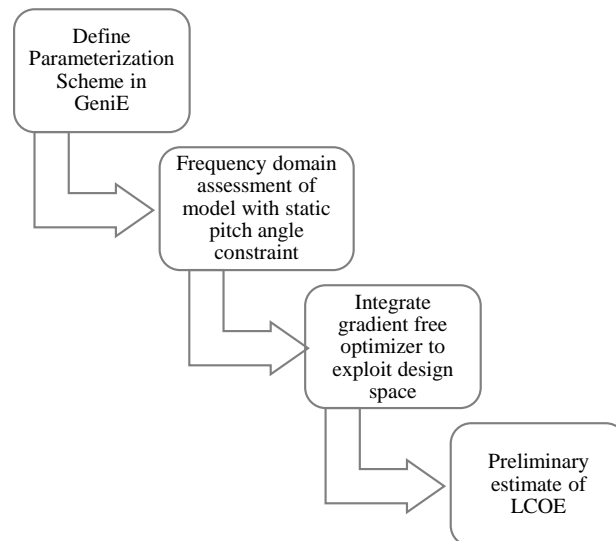




381 **3. Methodology and LCOE**

382 *3.1. Overview*

383 The majority of wind turbines are rated according to their power output (Ramachandran et al., 2013), and each  
384 rated turbine has a unique rotor nacelle assembly design. To effect quick optimization changes on the FOWT  
385 system for economic feasibility purposes is best done on the substructures - platform, mooring and anchor designs.  
386 As highlighted in section 1, the cost of a FOWT platform is substantially more than the fixed-bottom design  
387 configuration. It has been shown that the mass of steel used in the design of ship hull and FOWT platforms can  
388 be reduced in Birk and Clauss (2002) and Ojo et al. (2022a) respectively using shape parameterization techniques  
389 like NURBS and B-spline within an optimization framework. This reduction in the mass of steel material used in  
390 manufacturing the hull/platform substantially reduces the cost of the structure. For mooring optimization, Munir  
391 et al. (2021) showed that Floating wind turbines (FWTs) with shared mooring systems can be one of the most  
392 cost-effective solutions in reducing mooring costs and also mooring footprint on the seabed which invariably  
393 minimized the disruption or total loss of the Ocean biodiversity.  
394 The methodological approach selected in this study is to estimate the LCOE of a 30MW and 60MW wind farms  
395 using an optimized platform distinguished by applying static pitch angle constraints in the optimization process.  
396 The optimal platforms based on the constraints are utilized in hypothetical wind farms to compare the economic  
397 feasibility using the LCOE financial parameter.  
398 The process adopted is similar to the approach used in Ojo et al. (2022a) with an additional task of preliminary  
399 LCOE estimation added to the framework. The proposed methodology for the exploration, exploitation and  
400 preliminary LCOE estimation of a FOWT farm is to firstly define a parameterization scheme with a robust design  
401 space configuration using the B-spline / NURBS parameterization technique. This is followed by assessing the  
402 design models within the design space with frequency domain analysis tools - Sesam suite by DNV (Genie and  
403 HydroD/Wadam). The next stage is to integrate the analysis with the optimizer for optimal design selection for  
404 the 5 degrees, 7.5 degrees and 10 degrees static pitch angle. The last stage involves estimating the LCOE for a  
405 10MW Floating Offshore Wind Farm (FOWF) – 2 platforms for each optimal design selected with each static  
406 pitch angle constraint. For this preliminary assessment, the hydrostatic analysis is sufficient to estimate the mass  
407 of the optimal platform. The described methodological process is shown in Figure 1. The schematic configuration  
408 of the FOWF estimated is shown in Fig2abc.  
409  
410



411  
412  
413  
414

Figure 1: Platform shape optimization and LCOE estimation of a FOWF



415 *3.2. Hydrostatics for mass estimation*

416 The design and optimization of any type of floating offshore wind system must satisfy the stability requirement.  
 417 This needs a detailed hydrostatic assessment to ensure the floater provides enough buoyancy to support the turbine,  
 418 tower and mooring lines while also restraining the heave, roll and pitch motions within allowable limits. The  
 419 hydrostatic equations in pitch for the available stability mechanisms based on ballast, waterplane area and mooring  
 420 systems are represented with the buoyancy equations and the restoring equation highlighted in Eqns. (5) and (6)  
 421 respectively.

$$M_{Total} = \rho_w V \quad (5)$$

$$(\rho_w g I_y + F_b z_{CB} - F_w z_{CG} + C_{55,moor}) \theta = F_T (z_{hub} - z_{CB}) \quad (6)$$

422  
 423  
 424  
 425  
 426 Where  $M_{Total}$  is the total mass of the FOWT system which consists of the substructure components (platform,  
 427 mooring lines, ballast and anchors) and the superstructure components (tower and turbine),  $\rho_w$  is the water density  
 428 and  $V$  is the volume of the displaced fluid,  $g$  is the acceleration due to gravity,  $I_y$  is the second moment of area of  
 429 the initial waterplane area (within the approximation of small angle of inclination, the waterplane area remains  
 430 constant) with regards to the X axis,  $F_b$  is the buoyancy force,  $z_{CB}$  is the center of buoyancy (point at which the  
 431 resultant buoyancy forces on the body acts),  $F_w$  is the system's weight force,  $z_{CG}$  is the system's center of gravity  
 432 (Point at which the total systems weight  $C_{55,moor}$  is the contribution of the mooring stiffness to the pitch stiffness,  
 433  $\theta$  is the pitch inclination angle,  $F_T$  is the thrust force from the wind speed and  $z_{hub}$  is the hub height.  
 434 The expressions on the left-hand side of Eqn. (6) highlights the stability mechanisms within the FOWT system.  
 435 The first expressions highlight the water plane stability mechanism, the second and third expression represents  
 436 the ballast stability mechanism (Ioannou et al., 2020) while the fourth expression represents the mooring stability  
 437 mechanism (Collu and Borg, 2016). A schematic highlighting all the forces and reference points mentioned for a  
 438 representative spar FOWT system is shown in Figure 2.  
 439  
 440

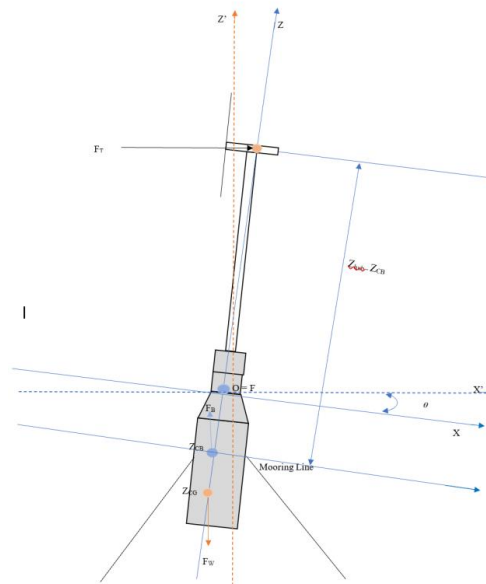
441 *3.3. Floatability and maximum inclination angle requirements*

442 The floatability requirement is satisfied with Eqn. (5) which highlights the equality of the buoyancy force of the  
 443 platform and the total mass of the substructure. With regards to the maximum angle of inclination, it is equivalent  
 444 to imposing a minimum pitch stiffness derived from Eqn. (6) and highlighted in Eqn.(7) (Ioannou et al., 2020).  
 445

$$\frac{F_T (z_{hub} - z_{CB})}{(\rho_w g I_y + F_b z_{CB} - F_w z_{CG} + C_{55,moor})} \leq \theta_{max} \quad (7)$$

Where  $(\rho_w g I_y + F_b z_{CB} - F_w z_{CG} + C_{55,moor})$  is the minimum total stiffness resulting in  
 the maximum angle of inclination.

446  
 447 The expression in Eqn. (7) is very important in the early stages of design as a constraint for exploring the design  
 448 space based on the allowable static pitch angle required for the FOWT system prior to conducting detailed analysis  
 449 on the design.  
 450  
 451  
 452  
 453



454  
455  
456

457 Figure 2: Sketch of forces and reference points of a representative spar FOWT.

458

#### 459 4. Techno-economic analysis, results and discussion

##### 460 4.1. Overview

461 As highlighted in section 2, the LCOE is an essential financial parameter for assessing any energy generating  
462 project – wind farms inclusive as it is the ratio of the costs of an energy project to the electricity production over  
463 its lifetime. A host of factors can reduce the LCOE amongst which are listed below and detailed in Markus Lerch  
464 (2019).

- 465 • CAPEX reduction due to optimization
- 466 • Cost reduction potential through industrialization
- 467 • Cost reduction due to economies of scale
- 468 • Cost reduction due to discount rate.

469

470 Exploring the four factors listed above will ensure the commercial viability of the FOWT concept and bring  
471 the LCOE cost for FOWT concepts down to what obtains in the fixed bottom offshore wind turbines. For the  
472 purpose of this study, the preliminary techno-economic assessment is based on the CAPEX reduction due to  
473 optimization. The CAPEX cost this study influences is the cost of the platform which makes up about 30% of the  
474 total CAPEX cost of a floating wind project (Shields et al., 2021). The shape of the platform is geometrically  
475 optimized with the objective of reducing the mass of steel used which invariably should reduce the cost of steel.  
476 The technicality involved in the shape optimization is highlighted in section 4.2. The effect of mass reduction of  
477 steel for platform development is highlighted in section 4.3.

478

##### 479 4.2. Technical Assessment

480 A high-level numerical simulation from a reference FOWT model (NREL OC3 spar platform) is assessed  
481 within a multidisciplinary design analysis and optimization framework to explore, exploit and select optimal



482 design variants from the design space. The optimal design variants are then assessed with a preliminary economic  
 483 feasibility study using a representative wind farm with material and cost assumptions from literature.  
 484

485 *4.2.1. Reference Design*

486 The reference design for this study is the OC3 spar platform supporting a conventional three-bladed, upwind  
 487 variable-speed 5MW baseline horizontal axis wind turbine. The geometric and structural properties of the OC3  
 488 spar platform is highlighted in Table 3 and Table 4 respectively.  
 489  
 490

Table 3: Geometric parameters for OC3 Spar (Jonkman, 2010)

Parameters	Dimensions (m)
Top cylinder diameter	6.5
Height of top cylinder	4
Diameter at top of transition area	6.5
Diameter at base of transition area	9.4
Height of transition area	8
Bottom cylinder diameter	9.4
Bottom cylinder height	108
Distance of platform keel to still water level (Draft)	120

491  
 492

Table 4: Floating platform structural properties (Jonkman, 2010)

Parameters	Values per Literature
Platform mass (including ballast) - (kg)	7,466,330
Center of mass below Sea water level (SWL) – (m)	89.9155
Platform roll inertia- about center of mass – kgm <sup>2</sup>	4,229,230,000
Platform pitch inertia- about center of mass – kgm <sup>2</sup>	4,229,230,000
Platform yaw inertia- about central axis – kgm <sup>2</sup>	164,230,000

493

494 *4.2.2. Technical Selection of optimal variants within an MDAO framework*

495 This study assesses a high-level hydrostatic study of a spar substructure discipline in a FOWT system. The  
 496 design is conducted using the B-Spline shape parameterization technique to enable the exploration of a rich design  
 497 space for optimal variant selection. B-spline is utilized due to its capability to alter the shape of the design locally  
 498 when the control point values are changed. This gives the designer an effective control of the shape with the  
 499 capability of exploring a richer design space. A metaheuristic pattern search optimization algorithm is used to  
 500 select the optimal design satisfying the specified objective function and constraints provided within the  
 501 optimization framework. The specified objective function in this study is minimizing the mass of the platform.  
 502 This objective is estimated by conducting a hydrostatic analysis using DNV suite – GeniE and WADAM stability  
 503 software. The process involved in the technical selection within the MDAO framework are detailed herein:  
 504

505 *4.2.2.1. B-Spline design of Spar.*

506 B-spline parameterization technique is selected for this study due to its many suitable properties amongst which  
 507 are: it has local propagation property for effective control of shape of a design, its capability to explore large and  
 508 rich design space, its invariance property under affine transformation and its quick simulation turnaround time.  
 509 Samareh (2001) showed that several low-degree Bezier segments can be used to represent a complex curve  
 510 rather than using a high degree Bezier curve. The resulting composite curve from this low degree representation  
 511 is a spline more accurately referred to as B-spline. A multisegmented B-spline is described in Eq. (8) (Samareh,  
 512 2001).  
 513

$$\bar{R}(u) = \sum_{i=1}^n \bar{P}_i N_{i,p}(u) \quad (8)$$

514



515 Where  $\bar{P}_i$  are the B-spline control points,  $p$  is the order/degree,  $N_{i,p}(u)$  is the  $i$ th B-spline basis function of  
 516 degree  $p$ . B-spline form can represent complex curves more efficiently and accurately than other curve  
 517 representation like the Bezier, cubic Hermite spline, cubic spline and polycurves.

518 This multi-segmented curve in Eqn. (8) is used in modelling the curve defining surface of the spar platform  
 519 used for the hydrostatic analysis of the FOWT system's substructure. Modelling was conducted with the B-spline  
 520 tool in DNV Sesam GeniE software.  
 521

#### 522 4.2.2.2. Hydrostatics and Optimization.

523 The high-level hydrostatic and optimization assessment in this study is conducted synchronously to obtain the  
 524 optimal design. The hydrostatic assessment is based on the stability Eqns. (5) and (6) highlighted in section 3 in  
 525 which the buoyancy force of the spar from the volume of liquid it displaces is equivalent to the total mass of the  
 526 system while also considering the contribution of the stability mechanisms. Eqn. (6) is also evolved into Eqn. (7)  
 527 which is an assessment of the maximum static pitch angle of the system. This is an important parameter which is  
 528 used as a constraint in the optimization assessment of the optimal design variant.

529 The optimization algorithm used in this study is the pattern search method. Pattern search is a relatively  
 530 inexpensive but rather effective optimization technique (Findler et al., 1987). It is based on the heuristic of  
 531 repeating the best search direction in exploratory moves as long as the response function improves. It also has the  
 532 capability adequately dispersed and appropriate number of starting points – multi-start ability to overcome noise  
 533 and the danger of getting trapped in local optima.

534 The optimization problem for this study is represented with the Eqn. (9).  
 535

$$\begin{aligned}
 & \min_{x \in \mathbb{R}} J(x) \\
 & \text{subject to } \begin{cases} x_{lower} \leq x \leq x_{upper} \\ h_i(x) = 0; i = 1 \text{ to } m \\ g_j(x) \leq 0; j = 1 \text{ to } p \end{cases} \quad (9)
 \end{aligned}$$

536 Where  $x$  is a  $k$ -dimensional vector of design variables with lower and upper bounds,  $J(x)$  is a single objective  
 537 function,  $m$  is the number of equality constraints and  $p$  is the number of inequality constraints. The main objective  
 538 for this optimization study is to minimize the mass of steel and invariantly, cost of the steel material used for the  
 539 spa platform. The two main constraints considered for all the parametric free-form curves considered in this study  
 540 are highlighted below:  
 541

- 542 1. Three maximum static pitch angles of inclination of the system set at 5 degrees, 7 degrees and 10 degrees  
 543 respectively.
- 544 2. A positive ballast mass to ensure floatability requirement.

545 The control points on the B-spline curve in Sesam GeniE are interfaced with the optimization algorithm with  
 546 python codes to ensure that design variables within the specified boundary conditions in the optimizer are passed  
 547 into Sesam Genie Java Script without human intervention. This ensure the static pitch angle constraint highlighted  
 548 in Eqn. (7) is coded into the optimization framework to integrate the hydrostatic analysis and the optimization  
 549 algorithm for feasible optimal design selection.

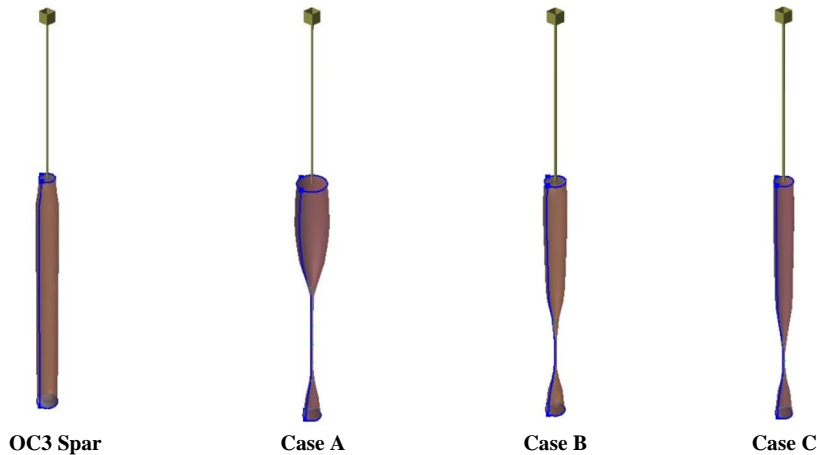
550 The optimal design variables obtained for the 12 segmented spar with 13 control points and a modelled OC3  
 551 spar with its dimension from literature are highlighted in Table 5 . The optimal variants in Table 5 based on the  
 552 static pitch constraints of 5 degrees, 7 degrees and 10 degrees are named case A, case B and case C respectively.  
 553 The model visuals from Sesam GeniE are presented in Figure 3 and it can be seen that the each of the three  
 554 optimized spars shows distinct geometric changes in comparison to the OC3 spar.  
 555



Table 5. Design data for selected models and OC3 spar

OC3 (m)	Height	0	4	12	30	40	50	60	70	80	90	100	110	120
	Radius	3.25	3.25	4.7	4.7	4.7	4.7	4.7	4.7	4.7	4.7	4.7	4.7	4.7
Case A (m)	Height	0	10	20	30	40	50	60	70	80	90	100	110	120
	Radius	6.91	6.86	7.22	6.04	5.00	0.55	0.50	0.50	0.50	0.50	0.53	3.38	3.92
Case B (m)	Height	0	10	20	30	40	50	60	70	80	90	100	110	120
	Radius	4.13	4.92	4.69	4.42	4.18	3.95	3.48	0.72	0.50	0.50	0.50	4.05	4.18
Case C (m)	Height	0	10	20	30	40	50	60	70	80	90	100	110	120
	Radius	3.72	4.13	4.01	3.89	3.77	3.65	3.54	2.64	0.50	0.50	0.50	3.65	3.71

556  
 557  
 558



559  
 560  
 561  
 562  
 563  
 564  
 565  
 566  
 567  
 568  
 569  
 570  
 571

Figure 3: Optimal models from pattern search optimization algorithm and OC3 spar

For each case in Figure 3, the models are constructed using B-Spline curves, and a material density of 7850 kg/m<sup>3</sup> (Steel) is used. A wall thickness of 0.0418 m is determined by utilizing the ratio of steel mass to buoyancy mass of 0.13, as highlighted in Anaya-Lara et al. (2018); Bachynski and Collu (2019). This wall thickness is selected based on the buoyancy mass of the NREL OC3 platform as a target value. Once the model is completed, Sesam Genie is utilized to generate finite element mesh (FEM) files to be used for their hydrostatic assessment.

Hydrodynamic analyses for the four cases are carried out using the Wave Analysis by Diffraction and Morison theory (Wadam) tool within the HydroD software of the DNV Sesam suite. The total mass of the system (including wind turbine, support platform, and ballast) and the system's center of gravity are determined through the Wadam analysis.

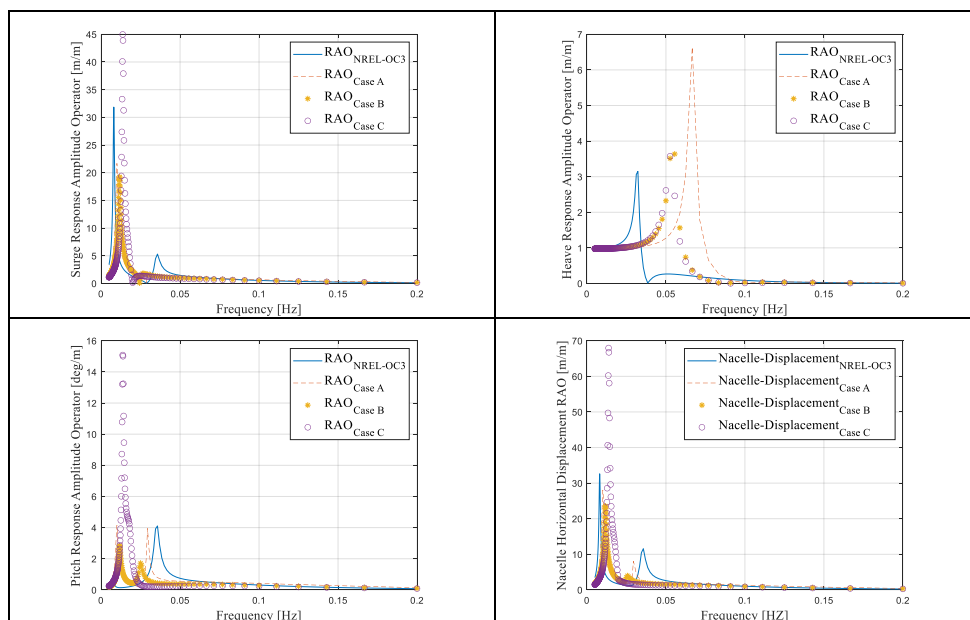
#### 4.2.2.3. Optimal Variants and Hydrodynamic Response

This section focuses on the inherent design characteristics of the model, specifically the system's responses. These responses are assessed with WADAM within DNV Sesam HydroD software. The assessment was conducted in a wave height of 2 meters (1 meter wave amplitude) and a time period of 5 seconds to 200 seconds in steps of 1 second. These responses are evaluated for all three cases and are compared to the OC3 NREL 5MW FOWT system. Figure 4 shows the Response Amplitude Operators (RAOs) in surge, heave, pitch, and horizontal nacelle displacement motion for the three design variant cases and the OC3 spar-buoy. The RAOs in Figure 4 shows the frequencies of the peak motion response of the system. This is a very important tool for subsequent design of the system in different environmental conditions to ensure the system's response avoid these peak motion response frequencies.



582 From an operational perspective, case C is projected to display the highest motion across all considered degrees  
 583 of freedom (DOFs), except for the heave DOF where case A exhibits the greatest motion. In addition, the peak  
 584 frequencies of the platform variants are all outside the first order wave excitation frequency range of 0.05Hz to  
 585 0.2Hz (5-25 Seconds) in the surge, pitch and nacelle displacement responses. However, all the variants peak  
 586 periods are slightly within the first order wave excitation frequency range in the Heave degree of freedom. This  
 587 observation necessitates structural assessment for future work. While increasing the static pitch angle can  
 588 potentially reduce the steel material used for manufacturing, it can have consequences for the fatigue loads in the  
 589 tower as detailed in Souza and Bachynski-Polić (2022). The authors conducted fatigue assessment on three 20MW  
 590 spar FOWTs with static pitch angles of 6, 8 and 10 degrees. They concluded that for a 20MW FOWT, the largest  
 591 fatigue damage at the still waterline was observed on the platform with 10 degrees static pitch angle. However,  
 592 for the tower, the design with the 6 degrees static pitch angle resulted in increased fatigue damage.

593 In addition, to the need for structural assessment, manufacturing can also be a challenge. However,  
 594 technologies like Metal 3D printing and concrete slip-forming can potentially resolve manufacturing issues of the  
 595 bespoke shaped spar.  
 596  
 597  
 598



599  
 600 Figure 4. Surge, Heave, Pitch and Nacelle displacement RAO

601  
 602

603 *4.3. Economic Feasibility study*

604 Some of the financial parameters used in assessing various projects in literature are highlighted in section 2.  
 605 However, for the purpose of this study, the financial parameter chosen to assess the economic feasibility of the  
 606 project to assess in this study is the LCOE.

607 The wind farm site used to assess the LCOE for this study is the Hywind wind park with a hypothetical water  
 608 depth of 320m. It is essential to utilize measured data for the annual energy production (AEP) estimation of the  
 609 project site. For this article, the AEP estimate of the Hywind site is taken from Saenz-Aguire et al. (2022) where  
 610 they have used the conventional Weibull distribution based calculation for the estimated energy generation at the  
 611 site during a studied climate period between 1991 and 2020. Their calculations are summarized as a fitting of the  
 612 shape parameter 'k' and scale parameter 'c' related to the Weibull distribution to match the 30-year wind speed



613 data, and a latter implementation of the power curve of the FOWT on the fitted histogram to estimate its energy  
614 production. Based on the work done in Saenz-Aguirre et al. (2022), the AEP value for the study is 139.8 GWh.  
615 Based on the AEP value of 23.2 GWh for a FOWT, the capacity factor worked out from a name-plate wind farm  
616 of 30 MW is 52.97%. The capacity factor of 52.97% estimated from this study is much more conservative than  
617 the AEP capacity factor of 65% recorded for the HyWind Scotland floating wind farm site in Aldersey-Williams  
618 et al. (2020).  
619

#### 620 4.3.1. CAPEX OPEX and DECEX Estimation

621  
622 Due to the large number of cost components and frequent difficulty and complexity of the FOWT system, the  
623 Capital Expenditure (CAPEX) for a Floating offshore wind farm (FOWF) is challenging to quantify. According  
624 to studies done like the Carbon Trust in 2015 (James, 2015) and projects completed and some currently under  
625 construction like HyWind Scotland, Kincardine Offshore wind farm, Windfloat Atlantic and HyWind Tampen,  
626 the main cost items are related to turbines, towers, platforms, moorings, anchors and the balance of the system,  
627 amongst which are the cost of installation of the components that makes up the holistic system, cost of the  
628 electrical grid and connections to shore.

629 As highlighted in Maienza et al. (2020), CAPEX contributions are mostly determined analytically and /or as a  
630 function of the wind farm's installed power. The costs for components and installations are taken into account  
631 separately, in part because the former is moderately dependent on the site of installation while the latter heavily  
632 depends on the site of installation. The CAPEX is the largest cost and it includes all investment costs to be faced  
633 before the commercial operation date (Maienza et al., 2022). The contributions to OPEX are also calculated  
634 analytically and /or as a function of the installed power of the wind farm while contributions to DECEX  
635 (decommissioning and clearance) are calculated as a percentage of the installation procedures cost (Maienza et  
636 al., 2020).

637 For this study, the CAPEX costs are going to be taken from literature and in cases where they are not available,  
638 assumptions are made. The percentage split of a spar FOWF's CAPEX, OPEX and DECEX for this study is 77%,  
639 19% and 4% respectively as specified for a spar FOWF in Maienza et al. (2020).

640 The masses of the spar platform and corresponding estimated costs based on the platforms masses is shown in  
641 Table 6. The mass of the optimal design variant tends to reduce as the static pitch angle is increased as highlighted  
642 in Table 6 where the static pitch angle 5 degrees – Case A, 7 degrees – Case B and 10 degrees – Case C yielded  
643 reduced platform masses respectively. The reduction in the platform's mass based on the design and optimization  
644 constraints leads to a reduction in total cost of the wind farm as subsequently discussed in this section.

645 The estimation of the costs and assumptions made based on references from literature are presented in Table 7  
646 while the total cost estimate for the hypothetical 30MW Hywind site based on the variation in cost of the platform  
647 due to the static pitch angles are presented in Table 8 to Table 11. Similarly, a sensitivity study is conducted for a  
648 larger FOWF site – 60 MW farm to assess the total cost estimate for the OC3 platform and the optimal design  
649 variants based on the selected constraints and data presented in Table 14 to Table 17 in Appendix A.

650 A clear trend of results from Table 8 to Table 11 shows that the Hywind farm with the OC3 platform has the  
651 largest total cost and this is partly due to the observation made in Leimeister et al. (2020b) that the OC3 spar  
652 floater is highly over-dimensioned for safety reason; hence, more material cost for the platform, which impacts  
653 the total cost of the wind farm as highlighted in Table 8. The total cost estimates of the wind farms in Table 9 to  
654 Table 11 shows the static pitch angle constraint used within the design and optimization framework highlighted  
655 in section 4.2 has the capability of reducing or increasing the mass of the optimal design variant. The increase or  
656 decrease in the mass of the optimal platform's design variant is proportional to an increase or decrease in the cost  
657 of steel material for the platform and a cumulative effect of the cost increase or decrease is seen in a sample  
658 windfarm as highlighted in Table 8 to Table 11. The same observation is made on a larger FOWF i.e., the larger  
659 the static pitch angle, the smaller the mass of the platform and hence the total cost of material which significantly  
660 contributes to the total cost of the farm. The impact of the static pitch angle design constraint on the LCOE of the  
661 farm is discussed in section 4.3.2.  
662  
663

Table 6. Platform mass and corresponding cost estimate

Platform Type	Mass (Tonnes)	Cost- Steel (GBP)
OC3	1069.86	1.50E+06
Case A	811.29	1.14E+06
Case B	781.84	1.09E+06
Case C	736.55	1.03E+06





664  
665

Table 7. Assumptions for hypothetical Hywind wind farm (30 MW – 6 Turbines)

CAPEX Components	Assumption	Unit	Reference
Turbine	1.3	[million GBP/MW]	(Ghigo et al., 2020)
Platform	Material cost.f	[million GBP]	(Maienza et al., 2020; Ghigo et al., 2020)
Anchors	80000/ Anchor	[GBP]	(James, 2015)
Moorings	500	[GBP/m]	(Myhr et al., 2014)
Export marine cables	400	[GBP/m]	(Ghigo et al., 2020)
Array marine cables	600	[GBP/m]	(Ghigo et al., 2020; Maienza et al., 2020)
Installation	1.5	[m GBP/MW]	(James, 2015)
Offshore electrical substation	3312000	[million GBP]	Scaled from Maienza et al. (2020)
Onshore electrical substation	1653600	[million GBP]	Scaled from Maienza et al. (2020)
OPEX			
Operating Expenditure	19% of Total Expenditure		(Maienza et al., 2020)
DECEX			
Decommissioning and clearing	4% of Total Expenditure		(Maienza et al., 2020)

666  
667

Table 8. Total cost for hypothetical Hywind wind farm (30 MW – 6 Turbines) – OC3 Platform

CAPEX Estimate (GBP)	171063720
OPEX Estimate (GBP)	42210528.31
DECEX Estimate (GBP)	8886427.013
Total Cost (GBP)	222160675.3

668  
669

Table 9. Total cost for hypothetical Hywind wind farm (30 MW – 6 Turbines) – 5<sup>0</sup> static pitch angle platform - CaseA

CAPEX Estimate (GBP)	160203780
OPEX Estimate (GBP)	39530802.86
DECEX Estimate (GBP)	8322274.286
Total Cost (GBP)	208056857.1

670  
671

Table 10. Total cost for hypothetical Hywind wind farm (30 MW – 6 Turbines) – 7<sup>0</sup> static pitch angle platform - CaseB

CAPEX Estimate (GBP)	158966880
OPEX Estimate (GBP)	39225593.77
DECEX Estimate (GBP)	8258019.74
Total Cost (GBP)	206450493.5

672  
673

Table 11. Total cost for hypothetical Hywind wind farm (30 MW – 6 Turbines) – 10<sup>0</sup> static pitch angle platform - CaseC

CAPEX Estimate (GBP)	157,084,700
OPEX Estimate (GBP)	38,756,225
DECEX Estimate (GBP)	8,159,205
Total Cost (GBP)	203,980,130

674  
675



676 4.3.2. LCOE Estimation

677

678

679

680

681

682

683

684

685

686

687

688

689

690

691

692

693

694

695

696

697

698

699

700

701

702

703

704

705

706

707

708

709

710

711

712

713

714

715

716

717

718

719

720

721

722

723

724

725

726

727

728

729

730

731

732

733

734

735

The levelized cost of energy (LCOE) calculation is the ratio of the net present value of total cost to the net present value of electricity generation. It is a method used to obtain the cost of one unit energy produced and is typically applied to compare the cost competitiveness of different power generation technologies and concepts (Markus Lerch, 2019). LCOE's results are based on the discounted values of CAPEX, OPEX and DECEX before being distributed relative to the energy generation (Myhr et al., 2014). LCOE returns the constant real energy price required to generate the return equal to the discount rate used over the full life of the project (Aldersey-Williams and Rubert, 2019).

The discount rate is a critical criterion in estimating the LCOE as the higher the discount rate, the larger the range of LCOE in the future and the lower the discount rate, the lower the LCOE in the future (Aldersey-Williams and Rubert, 2019). The discount rate typically presents values in the range of 8 % - 12 % for offshore wind investments (Martinez and Iglesias, 2022). For conservative purpose, this study is adopting a discount rate of 10% and the lifetime of the project is set to be 20 years.

For the purpose of this study, the CAPEX values are distributed as per the values in Table 8 to Table 11 for the 30 MW demonstration wind farm for the four varying optimal platform designs considered and in Table 14 to Table 17 in Appendix A for the 60 MW demonstration project considered for the different optimal platform designs considered. The OPEX costs are assumed to be evenly distributed over the 20 years of operation. The DECEX cost is assumed to be a one-off distribution process after the operation phase.

The mass of the designed platform tends to vary based on the design constraint specified as shown in Figure 5 and highlighted in Table 6 where the mass of the optimal platform variants reduces as the static pitch angle constraint is increased. The cumulative effect of the reduction in mass due to the design constraint on the total cost of the farm is discussed in section 4.3.1. However, the cumulative effect of the reduction in mass due to design constraint on the platform cost for 30 MW farm and 60 MW farm are highlighted in Table 12 and shown in Figure 6 and Figure 8 respectively. Table 12 shows that for both the 30 MW and 60 MW FOWFs, the total mass of the platforms used in both sides reduces as the static pitch angles are increased from 5 degrees to 7 degrees and 10 degrees respectively for both farms. This reduction in the mass of material – Steel used in manufacturing the designed platforms also culminates in the reduction in the cost of the materials used in manufacturing the platforms as detailed in Table 12 for both FOWFs. This occurrence (reduction in total mass of platform due to increase in static pitch angle) is also shown in Figure 6 and Figure 8 for the 30 MW and 60 MW FOWFs respectively.

The LCOE for the 30 MW site and the 60 MW site is developed based on the site's total costs for each optimal design highlighted in section 4.3.1 and Appendix A respectively. This study investigates the LCOE result from two fronts highlighted below:

1. The impact of the design constraint on the estimated LCOE of the FOWF.
2. The effect of scaling up a FOWF on the LCOE of the project.

The impact of the design constraint – mainly the static pitch angle on the LCOE is demonstrated on a 30 MW FOWF as highlighted in Table 13 and shown in Figure 7 where the LCOE for the 30 MW OC3 FOWF is the largest with a value of 197 £/MWh.

The LCOE values for the 30 MW FOWFs based on static pitch constraints of 5 degrees, 7 degrees and 10 degrees are 185 £/MWh, 183 £/MWh and 181 £/MWh respectively. The reduction in the LCOE is due to a cumulative effect of the mass reduction from optimizing a single platform on the six platforms carrying 5 MW NREL turbines that make up the floating wind farm. Although, the difference is not very significant, this result shows that the design optimization of a FOWT platform which is a component of the FOWT system contributes to the reduction in the LCOE of a FOWF.

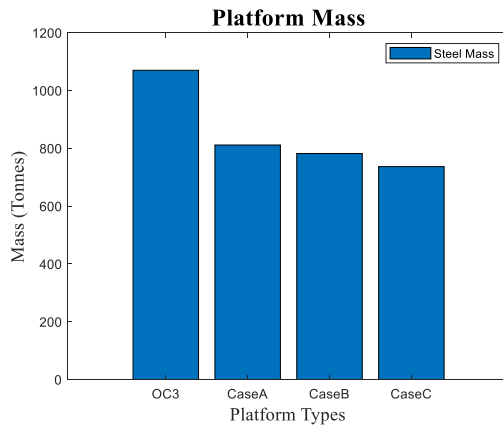
The study on the effect of scaling up the 30 MW FOWF is conducted by doubling its capacity to 60 MW. The LCOE result for the 60 MW FOWF is highlighted in Table 13 and shown in Figure 9. Just like the 30 MW FOWF, the LCOE for the 60 MW FOWF is the largest with a value of 185 £/MWh. The LCOE for the 60 MW OC3 platform FOWF is 6.23 % lower than the LCOE of the 30 MW OC3 platform FOWF.

The LCOE values for the 60 MW FOWFs based on static pitch constraints of 5 degrees, 7 degrees and 10 degrees are 176 £/MWh, 175 £/MWh and 173 £/MWh respectively. Table 13 shows the difference between 5 degrees, 7 degrees and 10 degrees static pitch angle constraint design variants of the 60 MW FOWF is 4.68 %, 4.72 % and 4.78 % lower than the corresponding optimal design variants for the 30 MW FOWF.

This significant reduction in LCOE values between the 60 MW FOWF and the 30 MW FOWF is a cumulative effect of the mass optimization of the platform as detailed in section 4.2 and the concept of scaling up the floating wind size (economies of scale). The concept of increasing the farm size is detailed in Myhr et al. (2014) where they showed that by increasing the number of turbines from 100 to 200 would lower the LCOE by approximately 10 % and that by increasing the turbines to 600 results in an LCOE reduction of up to 15 %. The reduction in the



736 LCOE value for the optimal design variants between the 60 MW and 30 MW FOWFs considered in this study is  
 737 less than 5 %. The 5 % reduction in LCOE value is not as significant as the 10 % to 15 % reduction in LCOE  
 738 value recorded in Myhr et al. (2014). However, comparing the number of turbines - 200 it took Myhr et al. (2014)  
 739 to attain 10 % reduction in LCOE value with the 12 turbines we have used to attain about 5 % reduction in LCOE  
 740 value in this study, the approach adopted using platform mass optimization in combination with scaling up the  
 741 floating wind farm is a much more effective approach to reducing the value of the LCOE in comparison to just  
 742 scaling up the farm size or conducting platform mass optimization alone.  
 743



744  
 745  
 746 Figure 5: Mass of platform types

747 Table 12. Estimated total platform mass and total platform material cost for 30 MW and 60 MW FOWF

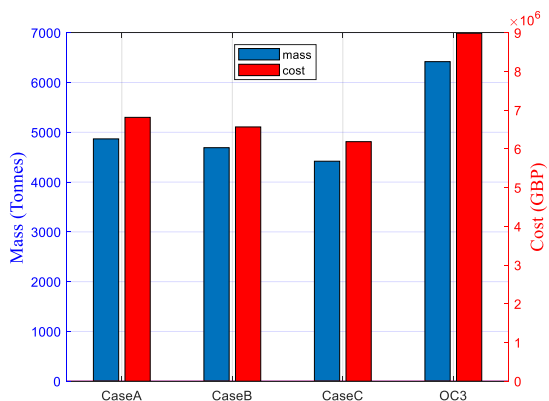
Design Variants	30 MW FOWF Platform mass (Tonnes)	60 MW FOWF Platform mass (Tonnes)	30 MW FOWF Platform cost (£)	60 MW FOWF Platform cost (£)
OC3 Design	6419.16	12838.32	8.99E+06	1.80E+07
Case A- 5 <sup>0</sup> Static Pitch angle	4867.74	9735.48	6.81E+06	1.36E+07
Case B- 7 <sup>0</sup> Static Pitch angle	4691.04	9382.08	6.57E+06	1.31E+07
Case C- 10 <sup>0</sup> Static Pitch angle	4419.3	8838.6	6.19E+06	1.24E+07

748  
 749

Table 13. LCOE comparison for 30 MW and 60 MW FOWF with 10% discount rate

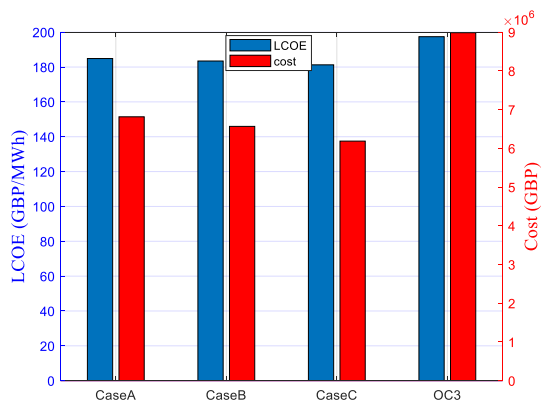
Design Variants	LCOE – 30 MW FOWF (£/MWh)	LCOE – 60 MW FOWF (£/MWh)	Percentage Difference (%)
OC3 Design	197	185	6.23
Case A- 5 <sup>0</sup> Static Pitch angle	185	176	4.68
Case B- 7 <sup>0</sup> Static Pitch angle	183	175	4.72
Case C- 10 <sup>0</sup> Static Pitch angle	181	173	4.78

750  
 751



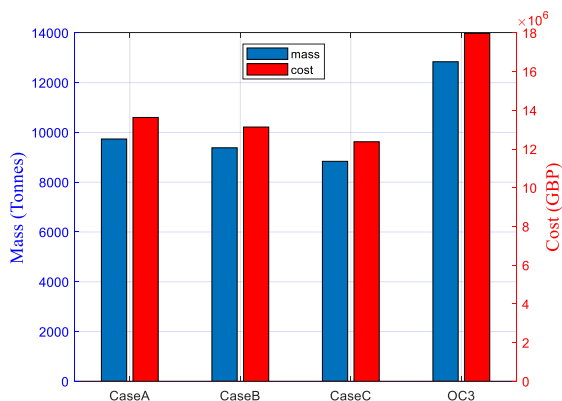
752  
 753 Figure 6: 30MW Farm Total Platform Mass and Total Platforms Material Cost

754  
 755



756  
 757 Figure 7: 30MW Farm LCOE and Total Platforms Steel Cost

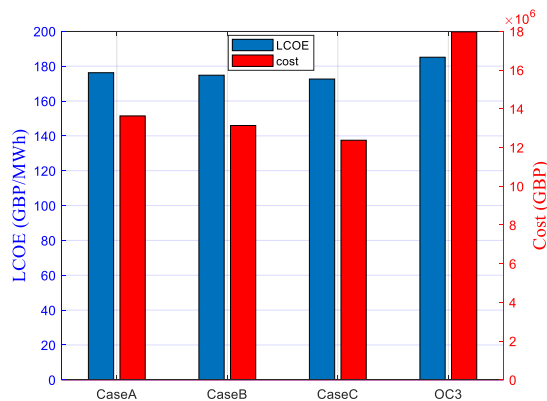
758



759  
 760 Figure 8: 60MW Farm Total Platform Mass and Total Platforms Material Cost



761  
762



763  
764

Figure 9: 60MW Farm LCOE and Total Platforms Steel Cost

765

## 766 5. Conclusion and recommendation

767 This study investigates the economic implication of use of bespoke geometric shape parameterization, design,  
768 analysis and optimization framework of spar platforms on a 30 MW floating wind farm and also the cumulative  
769 effect of this bespoke approach and economies of scale on a 60 MW floating wind farm. The bespoke technical  
770 assessment was conducted using the B-spline shape parameterization technique within an MDAO frame work to  
771 design analyze and optimize the concept. The shape parameterization and alteration of the design was conducted  
772 with Sesam Genie using B-Spline parameterization technique, analyses of the design was conducted using the  
773 hydrostatic capability of the Hydro D tools and optimization of the frame work was executed with the Pattern  
774 search (derivative free) optimization method. The main design constraint within the optimizer to facilitate the  
775 shape alteration within the MDAO framework is the static pitch angle. This study considered there static pitch  
776 angles of 5 degrees, 7 degrees and 10 degrees respectively and the OC3 NREL model. As highlighted in literature,  
777 the OC3 model is over-dimensioned for safety reasons; hence, it has the largest mass of all the optimal models  
778 considered. It is followed by the 5 degrees static pitch angled optimal model then the 7 degrees and 10 degrees  
779 static pitch angled optimal model respectively. This shows that as the static pitch angle is increased, the mass of  
780 the optimal platform model reduces. The mass reduction of the platform as a result of the constraints used in the  
781 design contributes to a reduction in material cost – a vital component of the total CAPEX cost for a FOWF.

782 The ratio of the net present value of total cost to the net present value of electricity generation which translates  
783 to the LCOE are the financial parameters used in assessing the different scenarios considered in this study (30  
784 MW FOWFs and 60 MW FOWFs for OC3 NREL platforms, 5 degrees, 7 degrees and 10 degrees static pitch  
785 constrained platforms). The LCOE values for the 30 MW FOWFs based on the OC3 platform model and static  
786 pitch constraints platform models of 5 degrees, 7 degrees and 10 degrees are 197 £/MWh, 185 £/MWh, 183  
787 £/MWh and 181 £/MWh respectively. On scaling up the farm size to 60 MW, the estimated LCOE values for the  
788 30 MW FOWFs based on the OC3 platform model and static pitch constraints platform models of 5 degrees, 7  
789 degrees and 10 degrees are 185 £/MWh, 176 £/MWh, 175 £/MWh and 173 £/MWh respectively - which is 6.23  
790 %, 4.68 %, 4.72 % and 4.78 % lower than the corresponding optimal design variants for the 30 MW FOWF. This  
791 is due to a combination of design shape parameterization and optimization framework utilized in this study and  
792 economy of scale.

793 Recommended future work from this study is the structural assessment of the bespoke shaped optimized spar  
794 subject to different environmental conditions as it has been highlighted in some work that increasing the static  
795 pitch angle tends to have consequences for the fatigue life of the tower. Manufacturing of bespoke shaped spar is  
796 a constraint that must not be overlooked. However, ongoing research in the advancement of wire arc additive  
797 manufacturing (WAAM), particularly in the 3D printing of metals, and the development of concrete slip-forming  
798 techniques are expected to potentially provide valuable solutions for overcoming this constraint.

799



800 This preliminary study shows that in addition to other means of ensuring FOWT technology is as economically  
 801 and technically viable as the fixed-bottom counterpart (platform upscaling, government subsidy, holistic system  
 802 MDAO), geometric shape design and optimization of FOWT platform is an effective method that can be used in  
 803 reducing the cost of floating wind farms.  
 804

## 805 6. Competing Interest

806 The contact author declared that none of the authors has any competing interests.

807  
 808

809 **Author Contributions:** Article structure and conceptualization, A.O, M.C and A.C; Design and shape  
 810 alteration Software A.O; Data curation, A.O; Optimization framework, A.O, M.C and A.C; Analyses and  
 811 Investigation, A.O and M.C; Writing – Original draft preparation, A.O; Writing, review and editing, M.C and  
 812 A.C; Project Supervision, MC and AC.

813 **Acknowledgement:** This work is conducted with the Renewable Energy Marine Structures (REMS) group at  
 814 the University of Strathclyde and the funding is provided by the Engineering and Physical Sciences Research  
 815 Council (EPSRC) UK (Grant no: EP/L016303/1).

816  
 817

## Appendix A

818 This appendix provides total estimated cost for the scaled up Hywind wind farm from 30 MW to 60 MW  
 819 highlighting the variation in total costs due to the design constraint as discussed in section 4.  
 820

Table 14. Total cost for scaled up Hywind wind farm (60 MW – 12 Turbines) – OC3 Platform

CAPEX Estimate (GBP)	320,827,440
OPEX Estimate (GBP)	79,165,212.47
DECEX Estimate (GBP)	16,666,360.52
Total Cost (GBP)	416,659,013

821  
 822

Table 15. Total cost for scaled up Hywind wind farm (60 MW – 12 Turbines)– 5<sup>0</sup> static pitch angle platform - CaseA

CAPEX Estimate (GBP)	305,407,560
OPEX Estimate (GBP)	75,360,307.01
DECEX Estimate (GBP)	15,865,327.79
Total Cost (GBP)	396,633,194.8

823  
 824

Table 16. Total cost for scaled up Hywind wind farm (60 MW – 12 Turbines) – 7<sup>0</sup> static pitch angle platform - CaseB

CAPEX Estimate (GBP)	302,933,760
OPEX Estimate (GBP)	74,749,888.83
DECEX Estimate (GBP)	15,736,818.7
Total Cost (GBP)	393,420,467.5

825  
 826

Table 17. Total cost for scaled up Hywind wind farm (60 MW – 12 Turbines) – 10<sup>0</sup> static pitch angle platform - CaseC

CAPEX Estimate (GBP)	299,129,400
OPEX Estimate (GBP)	73,811,150.65
DECEX Estimate (GBP)	15,539,189.61
Total Cost (GBP)	388,479,740.3

827  
 828



829 **Reference**

830

831 Aldersey-Williams, J. and Rubert, T.: Levelised cost of energy – A theoretical justification and critical assessment,  
832 Energy Policy, 124, 169-179, <https://doi.org/10.1016/j.enpol.2018.10.004>, 2019.

833 Aldersey-Williams, J., Broadbent, I. D., and Strachan, P. A.: Analysis of United Kingdom offshore wind farm  
834 performance using public data: Improving the evidence base for policymaking, Utilities Policy, 62, 100985,  
835 <https://doi.org/10.1016/j.jup.2019.100985>, 2020.

836 Anaya-Lara, O., Tande, J. O., Uhlen, K., and Merz, K.: Offshore Wind Energy Technology, John Wiley &  
837 Sons 2018.

838 Bachynski, E. E. and Collu, M.: Offshore support structure design, doi:10.1049/PBPO129E\_ch7, 2019.

839 Birk, L.: Parametric modeling and shape optimization of offshore structures, International Journal of CAD/CAM,  
840 6, 29-40, 2006.

841 Birk, L. and Clauss, G.: Parametric hull design and automated optimization of offshore structures, 10th Int.  
842 Congress of the Int. Maritime Association of the Mediterranean, Hellas, Greece,

843 Butterfield, S., Musial, W., Jonkman, J. M., and Scлавounos, P. D.: Engineering Challenges for Floating Offshore  
844 Wind Turbines,

845 Campos, A., Molins, C., Gironella, X., and Trubat, P.: Spar concrete monolithic design for offshore wind turbines,  
846 169, 49-63, 10.1680/jmaen.2014.24, 2016.

847 Castro-Santos, L., Martins, E., and Guedes Soares, C.: Cost assessment methodology for combined wind and  
848 wave floating offshore renewable energy systems, Renewable Energy, 97, 866-880,  
849 <https://doi.org/10.1016/j.renene.2016.06.016>, 2016.

850 Castro-Santos, L., Bento, A. R., Silva, D., Salvação, N., and Guedes Soares, C.: Economic Feasibility of Floating  
851 Offshore Wind Farms in the North of Spain, 10.3390/jmse8010058, 2020a.

852 Castro-Santos, L., Silva, D., Bento, A. R., Salvação, N., and Guedes Soares, C.: Economic feasibility of floating  
853 offshore wind farms in Portugal, Ocean Engineering, 207, 107393,  
854 <https://doi.org/10.1016/j.oceaneng.2020.107393>, 2020b.

855 Clauss, G. F. and Birk, L.: Hydrodynamic shape optimization of large offshore structures, Applied Ocean  
856 Research, 18, 157-171, [https://doi.org/10.1016/S0141-1187\(96\)00028-4](https://doi.org/10.1016/S0141-1187(96)00028-4), 1996.

857 Collu, M. and Borg, M.: Design of floating offshore wind turbines, in: Offshore Wind Farms: Technologies,  
858 Design and Operation, Elsevier Inc., 359-385, 2016.

859 DNV-GL: Floating Wind: The Power to Commercialize, 2020.

860 Dou, S., Pegalajar-Jurado, A., Wang, S., Bredmose, H., and Stolpe, M.: Optimization of floating wind turbine  
861 support structures using frequency-domain analysis and analytical gradients, Journal of Physics: Conference  
862 Series, 1618, 042028, 10.1088/1742-6596/1618/4/042028, 2020.

863 Filgueira-Vizoso, A., Castro-Santos, L., Iglesias, D. C., Puime-Guillén, F., Lamas-Galdo, I., García-Diez, A. I.,  
864 Uzunoglu, E., Díaz, H., and Soares, C. G.: The Technical and Economic Feasibility of the CENTEC Floating  
865 Offshore Wind Platform, 10.3390/jmse10101344, 2022.

866 Findler, N. V., Lo, C., and Lo, R.: Pattern search for optimization, Mathematics and Computers in Simulation, 29,  
867 41-50, [https://doi.org/10.1016/0378-4754\(87\)90065-6](https://doi.org/10.1016/0378-4754(87)90065-6), 1987.

868 Ghigo, A., Cottura, L., Caradonna, R., Bracco, G., Mattiazzo, G., and Engineering: Platform Optimization and  
869 Cost Analysis in a Floating Offshore Wind Farm, Marine Science and Engineering, 8, 835, 10.3390/jmse8110835,  
870 2020.

871 GWEC: Floating Offshore Wind - A Global Opportunity, 2022.

872 Hall, M., Buckham, B., and Crawford, C.: Evolving offshore wind: A genetic algorithm-based support structure  
873 optimization framework for floating wind turbines, OCEANS 2013 MTS/IEEE Bergen: The Challenges of the  
874 Northern Dimension, 1-10, 10.1109/OCEANS-Bergen.2013.6608173,

875 Hegseth, J. M., Bachynski, E. E., and Martins, J. R.: Integrated design optimization of spar floating wind turbines,  
876 Marine Structures, 72, 102771, 2020.

877 Heronemus, W. E.: Pollution-free energy from the offshore winds, 8th Annual Conference and Exposition, Marine  
878 Technology Society, Washington, D.C. 1972.

879 Ioannou, A., Liang, Y., Jalón, M. L., and Brennan, F. P.: A preliminary parametric techno-economic study of  
880 offshore wind floater concepts, Ocean Engineering, 197, 106937,  
881 <https://doi.org/10.1016/j.oceaneng.2020.106937>, 2020.

882 IRENA: Renewable power generation costs in 2018, Abu Dhabi, 2019a.

883 IRENA: Future of wind. deployment, investment, technology, grid integration and socio-economic aspects, Abu  
884 Dhabi, 2019b.

885 James, R. C. R., M.: Floating Offshore Wind: Market and Technology Review, 79-93, 2015.

886 Jonkman, J. M.: Definition of the Floating System for Phase IV of OC3,

887 Kaldellis, J. K., Apostolou, D., Kapsali, M., and Kondili, E.: Environmental and social footprint of offshore wind  
888 energy. Comparison with onshore counterpart, Renewable Energy, 92, 543-556,



- 889 <https://doi.org/10.1016/j.renene.2016.02.018>, 2016.
- 890 Karimi, M.: Frequency domain modeling and multidisciplinary design optimization of floating offshore wind  
891 turbines, University of Victoria, 2018.
- 892 Karimi, M., Hall, M., Buckham, B., and Crawford, C.: A multi-objective design optimization approach for floating  
893 offshore wind turbine support structures, *Journal of Ocean Engineering and Marine Energy*, 3, 69-87,  
894 10.1007/s40722-016-0072-4, 2017.
- 895 Kikuchi, Y. and Ishihara, T.: Upscaling and levelized cost of energy for offshore wind turbines supported by semi-  
896 submersible floating platforms, *Journal of Physics: Conference Series*, 1356, 012033, 10.1088/1742-  
897 6596/1356/1/012033, 2019.
- 898 Leimeister, M., Kolios, A., and Collu, M.: Critical review of floating support structures for offshore wind farm  
899 deployment, *Journal of Physics: Conference Series*, 2018/10, 1-11, 10.1088/1742-6596/1104/1/012007,
- 900 Leimeister, M., Kolios, A., and Collu, M.: Development and Verification of an Aero-Hydro-Servo-Elastic  
901 Coupled Model of Dynamics for FOWT, Based on the MoWiT Library, 13, 1974, 2020a.
- 902 Leimeister, M., Bachynski, E. E., Muskulus, M., and Thomas, P.: Rational Upscaling of a Semi-submersible  
903 Floating Platform Supporting a Wind Turbine, *Energy Procedia*, 94, 434-442,  
904 <https://doi.org/10.1016/j.egypro.2016.09.212>, 2016.
- 905 Leimeister, M., Kolios, A., Collu, M., and Thomas, P.: Design optimization of the OC3 phase IV floating spar-  
906 buoy, based on global limit states, *Ocean Engineering*, 202, 107186,  
907 <https://doi.org/10.1016/j.oceaneng.2020.107186>, 2020b.
- 908 Lerch, M., De-Prada-Gil, M., Molins, C., and Benveniste, G.: Sensitivity analysis on the levelized cost of energy  
909 for floating offshore wind farms, *Sustainable Energy Technologies and Assessments*, 30, 77-90,  
910 <https://doi.org/10.1016/j.seta.2018.09.005>, 2018.
- 911 Maienza, C., Avossa, A. M., Picozzi, V., and Ricciardelli, F.: Feasibility analysis for floating offshore wind  
912 energy, *The International Journal of Life Cycle Assessment*, 27, 796-812, 10.1007/s11367-022-02055-8, 2022.
- 913 Maienza, C., Avossa, A. M., Ricciardelli, F., Coiro, D., Troise, G., and Georgakis, C. T.: A life cycle cost model  
914 for floating offshore wind farms, *Applied Energy*, 266, 114716, <https://doi.org/10.1016/j.apenergy.2020.114716>,  
915 2020.
- 916 Markus Lerch, J. A. N., Petter Andreas Berthelsen: Life50+ : D2.8 Expected LCOE for floating wind turbines  
917 10MW+ for 50m+ water depth, 2019.
- 918 Martinez, A. and Iglesias, G.: Mapping of the levelised cost of energy for floating offshore wind in the European  
919 Atlantic, *Renewable and Sustainable Energy Reviews*, 154, 111889, <https://doi.org/10.1016/j.rser.2021.111889>,  
920 2022.
- 921 Munir, H., Lee, C. F., and Ong, M. C.: Global analysis of floating offshore wind turbines with shared mooring  
922 system, *IOP Conference Series: Materials Science and Engineering*, 1201, 012024, 10.1088/1757-  
923 899X/1201/1/012024, 2021.
- 924 Myhr, A., Bjerkseter, C., Ågotnes, A., and Nygaard, T. A.: Levelised cost of energy for offshore floating wind  
925 turbines in a life cycle perspective, *Renewable Energy*, 66, 714-728,  
926 <https://doi.org/10.1016/j.renene.2014.01.017>, 2014.
- 927 Ojo, A., Collu, M., and Coraddu, A.: Parametrisation Scheme for Multidisciplinary Design Analysis and  
928 Optimisation of a Floating Offshore Wind Turbine Substructure – OC3 5MW Case Study, *Journal of Physics:*  
929 *Conference Series*, 2265, 042009, 10.1088/1742-6596/2265/4/042009, 2022a.
- 930 Ojo, A., Collu, M., and Coraddu, A.: Multidisciplinary design analysis and optimization of floating offshore wind  
931 turbine substructures: A review, *Ocean Engineering*, 266, 112727,  
932 <https://doi.org/10.1016/j.oceaneng.2022.112727>, 2022b.
- 933 Papi, F. and Bianchini, A.: Technical challenges in floating offshore wind turbine upscaling: A critical analysis  
934 based on the NREL 5 MW and IEA 15 MW Reference Turbines, *Renewable and Sustainable Energy Reviews*,  
935 162, 112489, <https://doi.org/10.1016/j.rser.2022.112489>, 2022.
- 936 Pham, T. D. and Shin, H.: A New Conceptual Design and Dynamic Analysis of a Spar-Type Offshore Wind  
937 Turbine Combined with a Moonpool, *Energies*, 12, 10.3390/en12193737, 2019.
- 938 Ramachandran, G., Robertson, A., Jonkman, J., and Masciola, M. D.: Investigation of response amplitude  
939 operators for floating offshore wind turbines, *The Twenty-third International Offshore and Polar Engineering*  
940 *Conference*,
- 941 Saenz-Aguirre, A., Ulazia, A., Ibarra-Berastegi, G., and Saenz, J.: Floating wind turbine energy and fatigue loads  
942 estimation according to climate period scaled wind and waves, *Energy Conversion and Management*, 271, 116303,  
943 <https://doi.org/10.1016/j.enconman.2022.116303>, 2022.
- 944 Samareh, J. A.: Survey of shape parameterization techniques for high-fidelity multidisciplinary shape  
945 optimization, *AIAA Journal*, 39, 877-884, 10.2514/2.1391, 2001.
- 946 Shields, M., Duffy, P., Musial, W., Laurienti, M., Heimiller, D., Spencer, R., and Optis, M.: The Costs and  
947 Feasibility of Floating Offshore Wind Energy in the O'ahu Region, United States, 10.2172/1826892, 2021.
- 948 Souza, C. E. S. d. and Bachynski-Polić, E. E.: Design, structural modeling, control, and performance of 20 MW





- 949 spar floating wind turbines, *Marine Structures*, 84, 103182, <https://doi.org/10.1016/j.marstruc.2022.103182>, 2022.  
950 Zheng, X. Y. and Lei, Y.: Stochastic response analysis for a floating offshore wind turbine integrated with a steel  
951 fish farming cage, *Applied Science*, 8, 1229, 2018.  
952